Hindawi
Mathematical Problems in Engineering
Volume 2022, Article ID 9646889, 11 pages
https://doi.org/10.1155/2022/9646889

Research Article

Parametric Study on Nonlinear Finite Element Analysis of Prestressed Reinforced Concrete Beam Strengthened by Fiber-Reinforced Plastics

Cindrawaty Lesmana,[1] **Hsuan-Teh Hu**,[2,3] **Tsun-Chen Pan**,[4] **and Zih-Shu Lin**[2]

[1]*Department of Civil Engineering, Universitas Kristen Maranatha, Bandung 40164, Indonesia*
[2]*Department of Civil Engineering, National Cheng Kung University, Tainan 701, Taiwan*
[3]*Department of Civil and Disaster Prevention Engineering, National United University, Miaoli 360, Taiwan*
[4]*Wenzao Ursuline University of Languages, Kaohsiung 807, Taiwan*

Correspondence should be addressed to Hsuan-Teh Hu; hthu@mail.ncku.edu.tw

Received 27 January 2022; Revised 10 May 2022; Accepted 28 May 2022; Published 16 June 2022

Academic Editor: Alfrendo Satyanaga

Finite element analysis has been commonly used in many studies to examine the performance of structural elements. The objective of this article is to assess the relevance of geometric and strengthened pattern uncertainty on prestressed reinforced concrete beams strengthened by fiber-reinforced plastics based on a nonlinear finite element analysis. The parametric study focuses on the significant effects of fiber-reinforced polymer, beam length, and prestressed load on the ultimate loading capacity of the prestressed reinforced concrete beam strengthened by fiber-reinforced plastics. The results demonstrate the advantages of fiber-reinforced plastics that significantly increase the stiffness and the ultimate loading capacity of prestressed reinforced concrete beams. It is found that the beams that are strengthened by the FRP with fibers oriented at 0° have better results than other orientation angles.

1. Introduction

Externally bonded FRP and its advantages have become an acceptable way of strengthening structural elements. The strengthening of existing reinforced concrete structures was successful to put up the structures to resist higher applied loads with minimal modifications to be made [1, 2]. Externally bonded FRP has become a preferable solution for strengthening if compared to the conventional way of using steel [3].

To investigate the strengthening of structural behavior, the appropriate constitutive models for the linear and nonlinear behaviors were essential to construct the structures in the first place. Each constitutive model affects the accuracy of the adequate results [4]. In nonlinear finite element analysis, it is necessary to have the right assumption of the nonlinear behavior of prestressed reinforced concrete (PC), such as cracking and plasticity of concrete, yielding of reinforcing steel, tension stiffening, and shear retention. The suitable modeling of the nonlinear behavior of FRP is critical in modeling the composite structure using finite element (FE) analysis [1].

FE has been used to produce a much more detailed set of results, and it is quicker and less expensive than experimental investigation. In this study, a failure analysis of the PC beams strengthened by externally bonded FRP was performed by ABAQUS. The parametric study is introduced to increase understanding of the relationships between input parameters and outcomes in strengthened PC Beams. The effects of beam length with different reinforcement ratios

and FRP configuration on the strengthened PC beams subjected to concentrated load are examined. In addition, the performance in strength and stiffness due to FRP is investigated, as well as the variation in the failure mechanisms of the beams.

2. Constitutive Models and Material Properties

2.1. Concrete. The concrete strain (ε_0) corresponding to the peak of stress f_c' was selected as 0.003 [5]. Poisson's ratio was assumed to be 0.2. The failure strengths of concrete under multiaxial combinations of loading are different from those observed under uniaxial conditions. According to Kupfer et al. [6], the maximum strength envelope under multiple stress conditions seems to be largely independent of the load path.

A Mohr–Coulomb type compression surface together with a crack detection surface to model the failure surface of concrete was adopted in ABAQUS. To model the existing crack, damaged elasticity was used. When plastic deformation occurs, a specific parameter should be defined to manage the expansion of the yield surface. Saenz's equivalent uniaxial stress-strain curve [7] is used for the nonlinear behavior of the concrete, as follows:

$$\sigma_c = \frac{E_c \varepsilon_c}{1 + (R + R_E - 2)(\varepsilon_c/\varepsilon_o) - (2R - 1)(\varepsilon_c/\varepsilon_o)^2 + R(\varepsilon_c/\varepsilon_o)^3}, \tag{1}$$

where $R = (R_E(R_\sigma - 1)/(R_\varepsilon - 1)^2) - (1/R_\varepsilon)$, $R_E = E_c/E_o$, $E_o = f_c'/\varepsilon_o$, and σ_c is an effective stress and ε_c is an effective strain; $R_\sigma = 4$ and $R_\varepsilon = 4$ are used [8].

2.2. Steel Rebar. The steel rebar is modelled as layers of equivalent thickness. The position, cross-sectional area, spacing, and orientation layer of the steel rebar need to be specified. The tension stiffening is introduced into the concrete cracking model so the transfer of load can be defined across the concrete cracks through the rebar. The elastic perfectly plastic was assumed to exemplify the stress-strain curve of the rebar with the yielding stress (f_{ys}) equal to 414 MPa. The elastic modulus of the rebar (E_s) was assumed to be 200 GPa. A Poisson's ratio of 0.3 was assigned for the rebar.

2.3. Prestressing Tendon. The nonlinear stress-strain curve was simplified into a piecewise linear curve for the tendon model. The elastic modulus of the prestressing tendon was assumed to be similar to that of the steel rebar, $E_s = 200$ GPa. The prestressing tendon was modelled as an equivalent uniaxial material which smeared through the element section and the specification of position, cross-sectional area, spacing, and each orientation layer of the tendon were defined.

2.4. Fiber-Reinforced Plastic. Each lamina is modelled as an orthotropic layer in a plane stress condition. The nonlinear strain-stress relation for a composite lamina behavior [9] is adopted to model the nonlinear in-plane shear behavior as follows:

$$\begin{Bmatrix} \varepsilon_1 \\ \varepsilon_2 \\ \gamma_{12} \end{Bmatrix} = \begin{bmatrix} \frac{1}{E_{11}} & -\frac{\nu_{21}}{E_{22}} & 0 \\ -\frac{\nu_{12}}{E_{11}} & \frac{1}{E_{22}} & 0 \\ 0 & 0 & \frac{1}{G_{12}} \end{bmatrix} \begin{Bmatrix} \sigma_1 \\ \sigma_2 \\ \tau_{12} \end{Bmatrix} + S_{6666} \cdot \tau_{12}^2 \begin{Bmatrix} 0 \\ 0 \\ \tau_{12} \end{Bmatrix}. \tag{2}$$

For the in-plane shear nonlinearity, only one constant, S_{6666}, is required to account for that determined by a curve fitted to various off-axis tension test data [9]. Define $\Delta\{\sigma'\} = \Delta\{\sigma_1, \sigma_2, \sigma_3\}^T$ and $\Delta\{\varepsilon'\} = \Delta\{\varepsilon_1, \varepsilon_2, \gamma_{12}\}^T$, invert and differentiate (2), and the incremental stress-strain relations for a nonlinear orthotropic lamina are established as follows:

$$\Delta\{\sigma'\} = [Q_1']\Delta\{\varepsilon'\},$$

$$[Q_1'] = \begin{bmatrix} \frac{E_{11}}{1 - \nu_{12}\nu_{21}} & \frac{\nu_{12}E_{22}}{1 - \nu_{12}\nu_{21}} & 0 \\ \frac{\nu_{21}E_{11}}{1 - \nu_{12}\nu_{21}} & \frac{E_{22}}{1 - \nu_{12}\nu_{21}} & 0 \\ 0 & 0 & \frac{1}{(1/G_{12}) - 3S_{6666}\tau_{12}^2} \end{bmatrix}. \tag{3}$$

The transverse shear stresses are assumed to behave linearly and do not affect the nonlinear behavior of any in-plane shear. Define $\Delta\{\tau_t'\} = \Delta\{\tau_{13}, \tau_{22}\}^T$ and $\Delta\{\gamma_t'\} = \Delta\{\gamma_{13}, \gamma_{22}\}^T$, and then the constitutive equation for transverse shear stresses becomes

$$\Delta\{\tau_t'\} = [Q_2']\Delta\{\gamma_t'\},$$

$$[Q_2'] = \begin{bmatrix} \alpha_1 G_{13} & 0 \\ 0 & \alpha_2 G_{23} \end{bmatrix}. \tag{4}$$

The terms α_1 and α_2 are the shear correction factors and are taken to be 0.83 [10].

The Tsai–Wu criterion [11] under plane stress conditions is adopted in this analysis as a failure criterion, as follows:

$$F_1\sigma_1 + F_2\sigma_2 + F_{11}\sigma_1^2 + 2F_{12}\sigma_1\sigma_2 + F_{22}\sigma_2^2 + F_{66}\tau_{12}^2 = 1, \tag{5}$$

with

$$F_1 = \frac{1}{\overline{X}} + \frac{1}{\overline{X'}},$$

$$F_2 = \frac{1}{\overline{Y}} + \frac{1}{\overline{Y'}},$$

$$F_{11} = \frac{-1}{\overline{X}\overline{X'}}, \tag{6}$$

$$F_{22} = \frac{-1}{\overline{Y}\overline{Y'}},$$

$$F_{66} = \frac{1}{\overline{S}^2}.$$

The $\overline{X}$, $\overline{Y}$ and $\overline{X}$', $\overline{Y}$' are the lamina longitudinal and transverse strengths in tension and compression, respectively, and $\overline{S}$ is the shear strength of the lamina. For practical engineering applications, F_{12} can be set equal to zero [12].

An incremental loading is applied to the composite beams until failures in one or more of the individual plies are indicated according to equation (5) during the numerical calculation. There are two rules to determine whether the ply failure is caused by resin fracture or fiber breakage [13]:

(1) If a ply fails but the stress in the fiber direction remains less than the uniaxial strength of the lamina in the fiber direction, the ply failure is assumed to be resin induced. As a result, the laminate loses its capability to support transverse and shear stresses but remains able to carry longitudinal stress. In this case, the constitutive matrix of the lamina becomes

$$[Q_1'] = \begin{bmatrix} E_{11} & 0 & 0 \\ 0 & 0 & 0 \\ 0 & 0 & 0 \end{bmatrix}. \quad (7)$$

(2) If a ply fails by σ_1 exceeding the uniaxial strength of the lamina, the ply failure is caused by fiber breakage, and a total ply rupture is assumed. In this case, the constitutive matrix of the lamina becomes

$$[Q_1'] = \begin{bmatrix} 0 & 0 & 0 \\ 0 & 0 & 0 \\ 0 & 0 & 0 \end{bmatrix}. \quad (8)$$

3. Parametric Study

To obtain the possible maximum ultimate load, the appropriate constitutive models for concrete, steel rebar, and tendons were implemented into ABAQUS, a finite element analysis program. A subroutine in the FORTRAN language is linked to the ABAQUS program to integrate the nonlinear constitutive equations of the FRP. The validity of all material models for concrete, steel, tendon, and FRP has been verified individually by testing against experimental data [14–16] and was not duplicated here.

Two beam models are analyzed in this study, a rectangular beam and a T-sectional beam. The model used in this study was a beam with cross section dimensions of 160 mm × 280 mm, as shown in Figure 1. For the T-beams, the slab contributory portion was taken as 80 mm from each beam side, and slab reinforcements were ignored due to their small effect. These T-beams were subjected to distributed load at the top surface of the beam as in Figure 1, with satisfied dimensions based on the requirements of the ACI code. The weight of the beams was neglected. For the strengthened material, carbon/epoxy AS4/3501-6 is used. Each FRP layer was 3 mm in thickness, and the tensile strength (X_{ut}) was 1860 MPa, while the elastic modulus (E_{11}) was 142 GPa. Since the FRP layers were only subjected to uniaxial tension in the fiber direction, these assumed parameters would not affect the uniaxial tensile behavior of the FRP. The following parameters were assumed to take the Tsai–Wu criterion into account: $E_{22} = 10.3$ GPa, $G_{12} = 6$ GPa, $X_{uc} = -1440$ MPa, $Y_{uc} = 57$ MPa, $Y_{ut} = -228$ MPa, $S_{6666} = 4.64 \times 10^{-25}$ MPa^{-3}, and υ_{12}. $X_{ut} = 0.21$.

The model beam had one plane of symmetry; thus, only half of the beam was analyzed, and symmetric boundary conditions were placed along the two symmetric planes. In the finite element analysis, 27-node solid elements (three degrees of freedom per node) are used to model the PC beams C3D20R. Based on the results of convergent elements, Table 1 shows the number of modelled elements that were used for analysis. The FRP is modelled by eight-node shell elements (six degrees of freedom per node) and directly attached to the outer surface of the PC beam (Figure 2).

3.1. Effect of Preloading Stress Variation on Pure Prestressed Concrete Beams. Three types of preloading stress are considered, 0.2 σ_p (260 MPa), 0.6 σ_p (780 MPa), and σ_p (1300 MPa). Figure 3 shows the load-displacement curves for rectangular long and short beams (R-long and R-short) and T-shaped long and short beams (T-long and T-short). With similar dimensions of width and height, the maximum loads of T-beams are slightly higher than those of rectangular beams. The higher the prestressed load, the higher the maximum load can be obtained, but the brittle structure in return.

For short beams, the maximum load is approximately doubled from the maximum load of long beams. The long beams are more ductile than the short PC beams, but the maximum load is relatively lower. Comparing the results of R-beams and T-beams, the higher maximum loads and displacement can be obtained by considering the slabs in the structure of beam elements.

The crack patterns in Figure 4 illustrate the crack element of prestressed concrete beams under maximum load. It is shown that the pattern of R-beams and T-beams tends to be similar. The failure of beams is affected by the length of beams and the amount of reinforcement. For long beams with lower prestressed load ($0.2\sigma_p$), the crack appears on the bottom at the center of the beams which indicates the occurrence of bending failure. The under-reinforced beam section undergoes a tensile failure, so the yielding of steel was responsible for continued higher strains in concrete, resulting in its failure. However, in the long beam with a higher prestressed load (σ_p) and the short beam prestressed load ($0.2\sigma_p$), the cracks appear both near the support and the center of the beams. The indication of crack in the support is always appeared from short PC beams. As shown in Figure 4, the cracks are shown at the corner for lower and higher prestressed loads. For short beams with higher prestressed load (σ_p), cracks appear only in the support. This indicates a higher prestressed load is effective to reduce the occurrence of bending failure.

3.2. Effect of the Number of FRP Layers on the Strengthened Prestressed Concrete Beams. The additional FRP layers would have significant effects on increasing the maximum load, especially for long beams (Figure 5). Figures 5 and 6

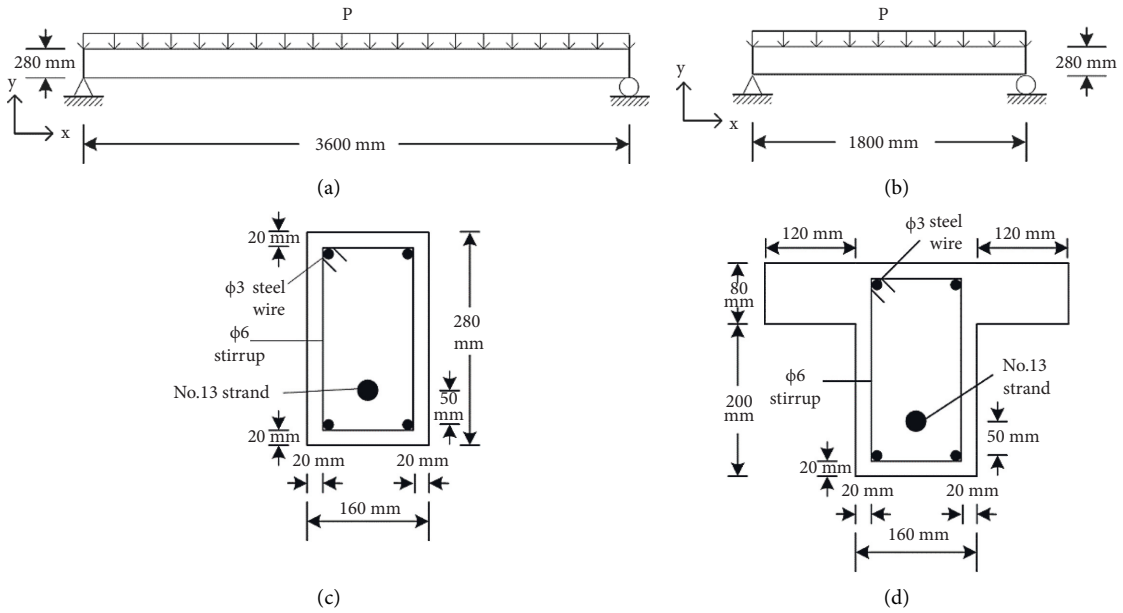

Figure 1: Prestress model for long and short PC beams.

Tabel 1: Mesh size of the PC beams model.

Type of beams		Total elements	Number of elements in direction		
			X	*Y*	*Z*
Rectangular	Long	510	34	5	3
	Short	255	17	5	3
T	Long	1840	46	3 (web) 7 (flange)	5
	Short	920	23	3 (web) 7 (flange)	5

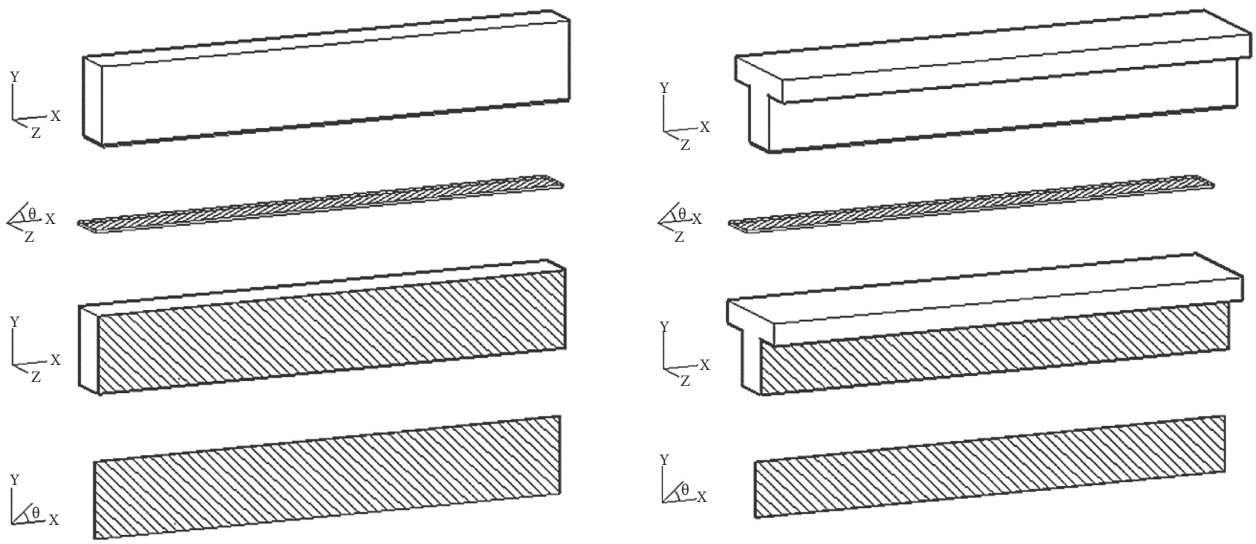

Figure 2: FRP illustration for parametric study of strengthened PC beams.

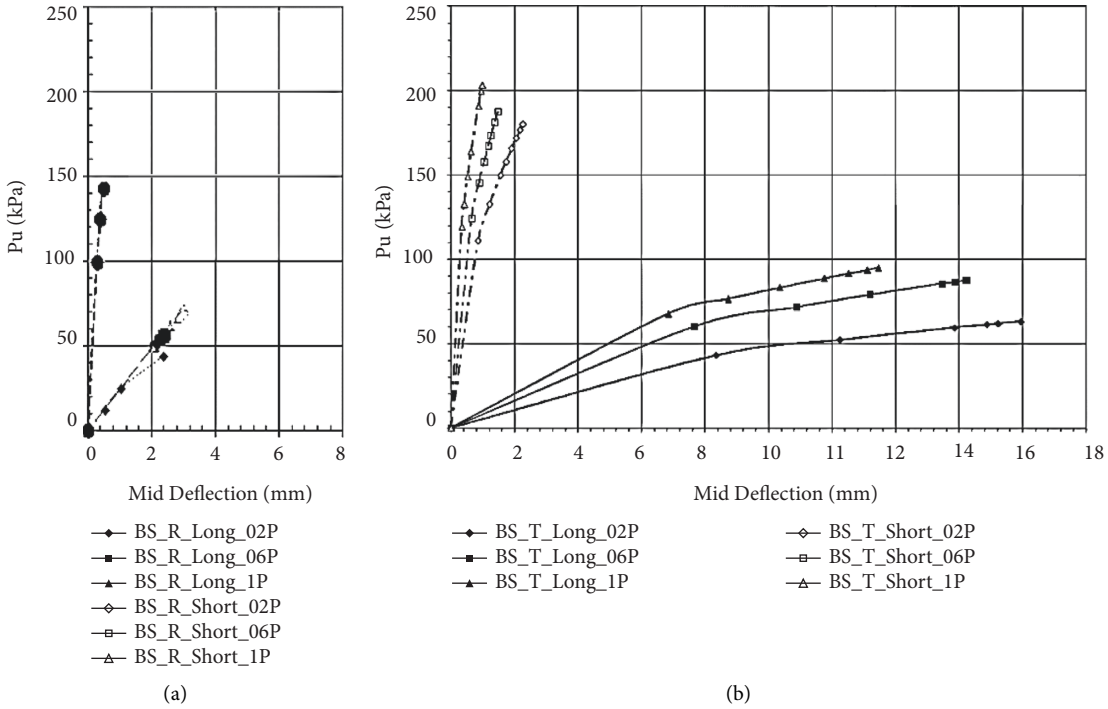

Figure 3: Load deflection curve for pure prestressed concrete beams. (a) Rectangular beam. (b) T-beam.

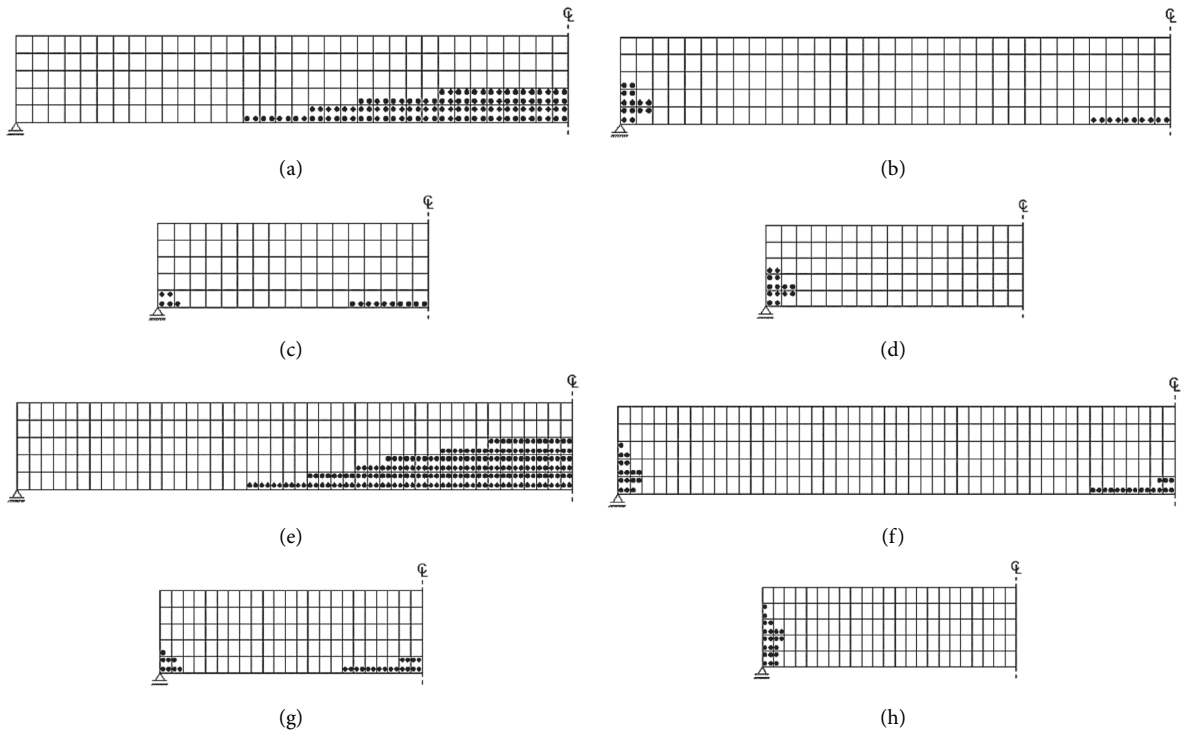

Figure 4: Crack pattern for prestressed concrete beams under maximum loading. (a) BS_R_Long_02P. (b) BS_R_Long_1P. (c) BS_R_Short_02P. (d) BS_R_Short_1P. (e) BS_T_Long_02P. (f) BS_T_Long_1P. (g) BS_T_Short_02P. (h) BS_T_Short_1P.

show the results of a various number of layers scenario with 0-degree fiber orientation. Comparing the results in Figure 5, T-shaped long beams have better ductility and maximum load.

Similar results can also be observed from short beams in Figure 6. The number of layers is increased with the maximum load and higher deflection compared to pure PC short beams. The stiffness of both long and short beams,

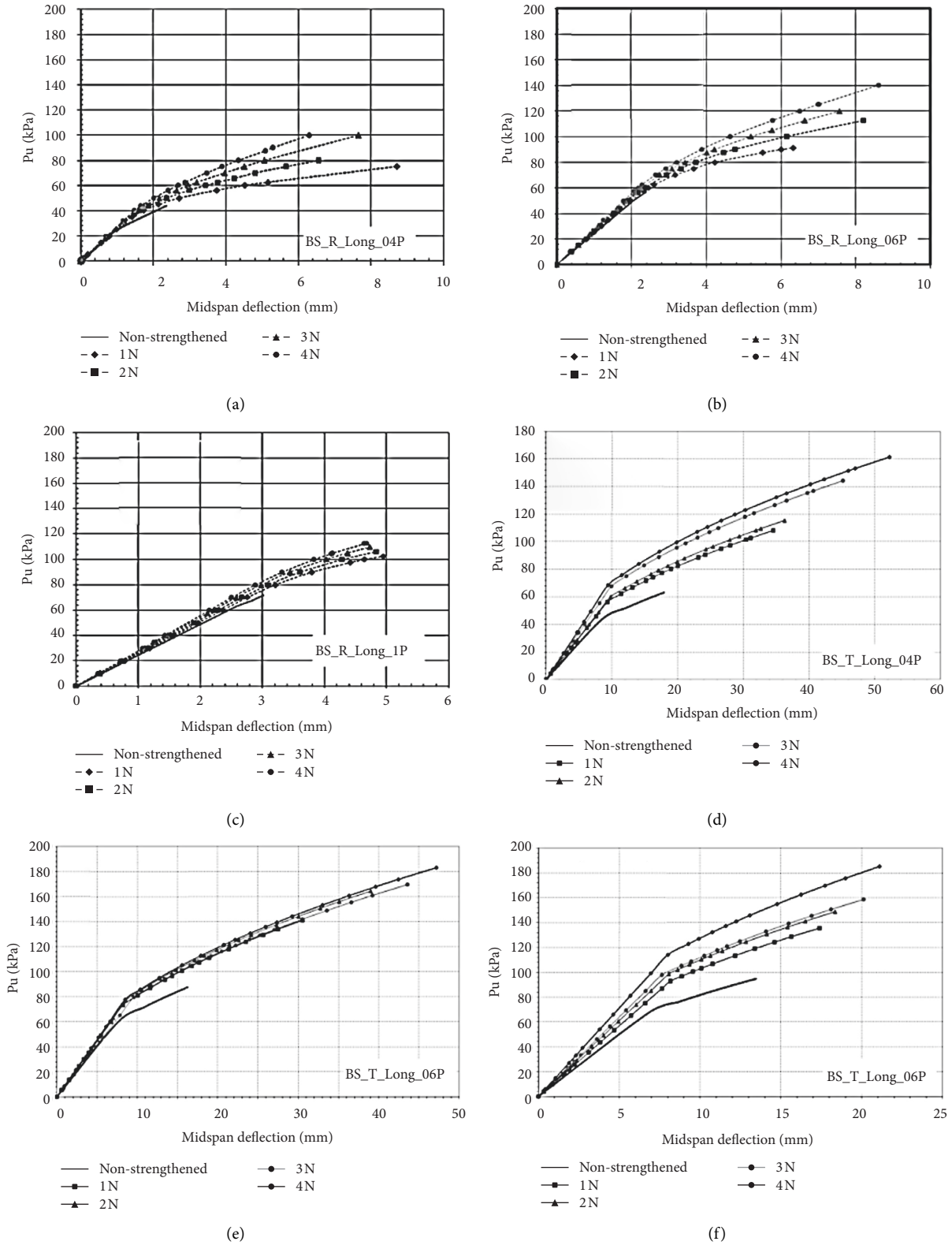

Figure 5: Load deflection curves for strengthened long prestressed concrete beams at the bottom for various number of layers. (a) R-beam $0.2\sigma_p$. (b) R-beam $0.6\sigma_p$. (c) R-beam σ_p. (d) T-beam $0.2\sigma_p$. (e) T-beam $0.6\sigma_p$. (f) T-beam σ_p.

represented by the gradient between load and deflection in each case, is slightly higher as the number of layers increased. The number of layers indeed can increase the strengthened effects between the PC and both rectangular and T-shaped beams, but due to the cost-effectiveness, the appropriate number of layers should be carefully estimated.

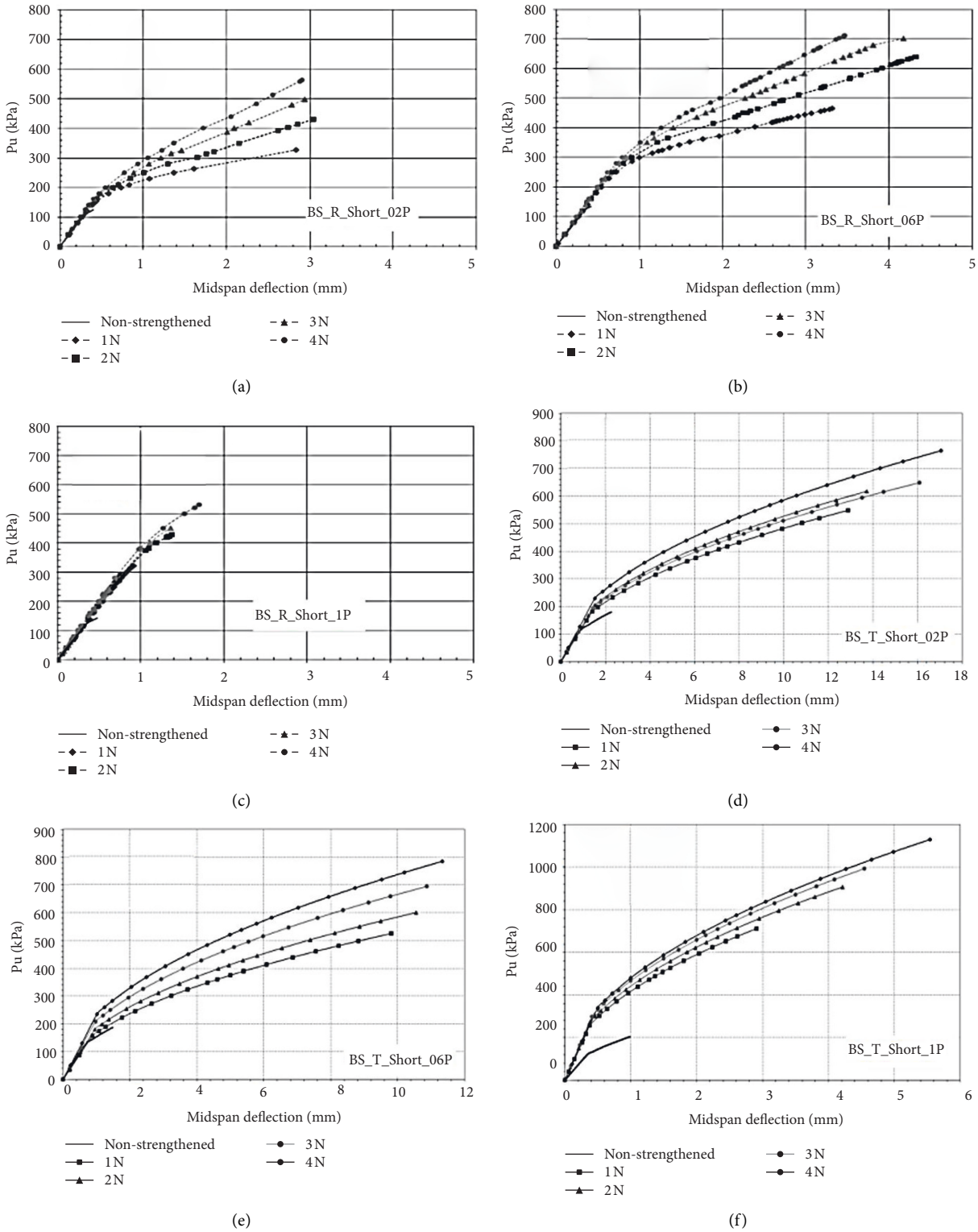

FIGURE 6: Load deflection curves for strengthened short prestressed concrete beams at the bottom for various number of layers. (a) R-beam $0.2\sigma_p$. (b) R-beam $0.6\sigma_p$. (c) R-beam σ_p. (d) T-beam $0.2\sigma_p$. (e) T-beam $0.6\sigma_p$. (f) T-beam σ_p.

The increase in the number of FRP layers would increase the maximum load (Figure 7). Comparing both shapes, the increased layers of T-beams have greater effects on increasing the maximum load. The strengthened effects are higher as the T-shaped is considered in the structure. The use of increased prestressed load is to increase the tensile strength of the structure. This benefit is similar to the increased number of layers. By adding two benefits in one

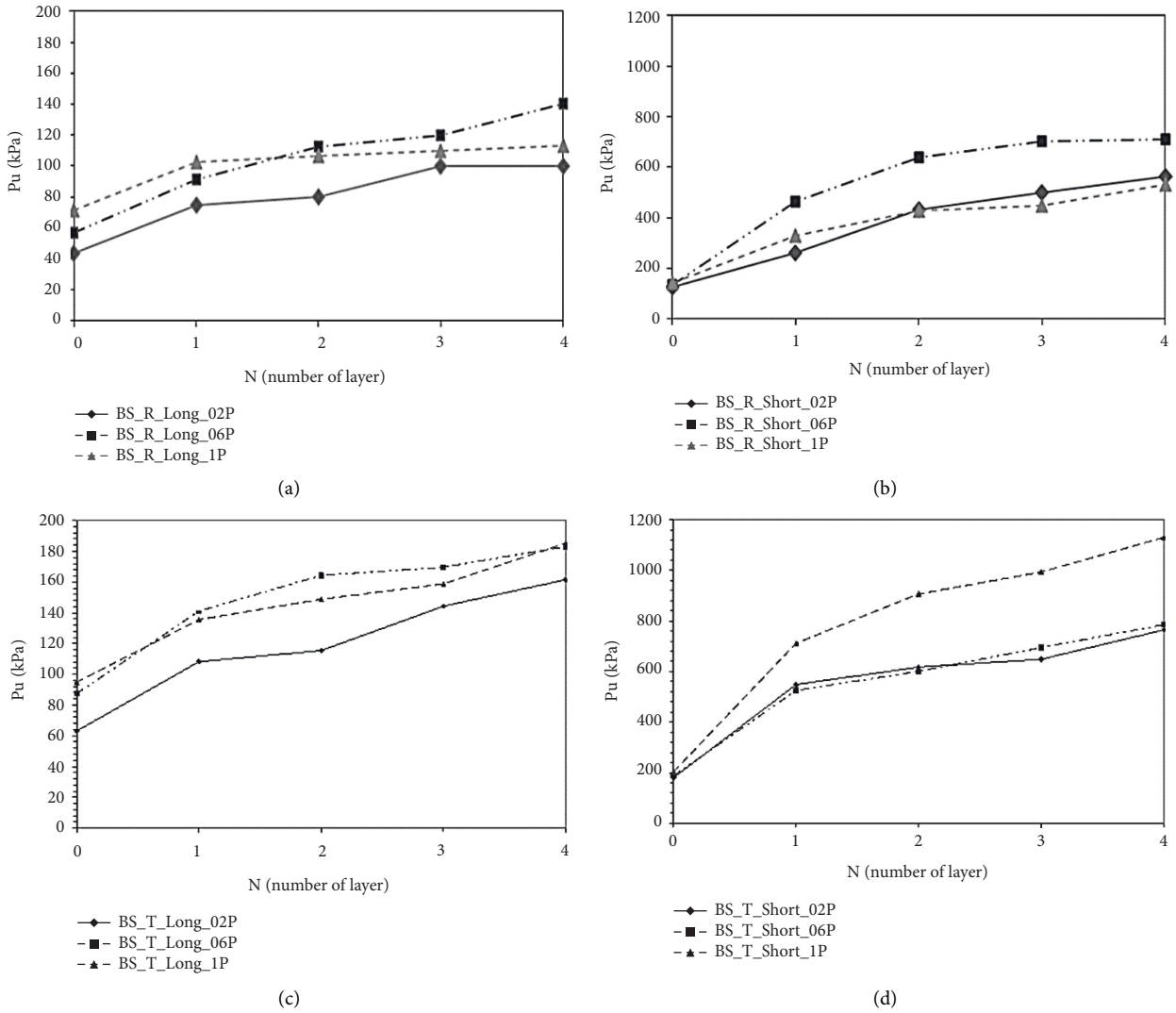

Figure 7: Relationship between number of layers and maximum load for strengthened PC beam. (a) R-beam (long). (b) R-beam (short). (c) T-beam (long). (d) T-beam (short).

element structure, the maximum load of strengthened PC beams becomes higher, but the increase in the load is only slightly significant.

The increased of the maximum load is significant with the additional layer of CFRP on the non-strengthened PC beam. For example,, without taking much consideration of the effect of prestressed load, the average increased maximum load on nonstrengthened to $N = 1$ is 50% for R-beam (long), 55% for T-beam (long), 150% for R-beam (short), and 200% for T-beam (short). For long beams with a lower prestressed load, $0.2\sigma_p$, the increased maximum loads for $N = 1$ to $N = 4$ are relatively small, 10% for R-beam (long) and 25% for T-beam (long). For long beams with higher prestressed loads, $0.6\sigma_p$ and σ_p, the increase in prestressed load is less significant compared to the increased number of layers. The increased maximum loads for $N = 1$ to $N = 4$ are approximately doubled from 55% to 125% for R-beam (long) and 60% to 120% for T-beam (long). Approximately similar results can be observed in short beams.

3.3. Effect of Fiber Orientation on the Strengthened Prestressed Concrete Beams. In this section, the CFRP is attached to both sides of the beam to increase the shear resistance of the PC beams. The thickness of each layer is similar, but the orientation of laminate lay-ups is modified into 5 cases: 0°, 30°, 45°, 60°, and 90°. The fiber angle of the lamina is measured counterclockwise from the midsurface of the beam.

In Figures 8 and 9, the results show that the different fiber orientations give different results in strengthening PC beams. The increased number of layers has a greater impact on the effect of fiber orientation to increase the maximum load. The effects of fiber orientation are more significant for both long and short beams with T-shapes subjected to lower prestressed loads. For long beams, as the number of layers is increased, the effects of fiber orientation are higher. On contrary, the effects of fiber orientation on the increased maximum load are more significant for short beams with a lower number of layers ($N < 2$).

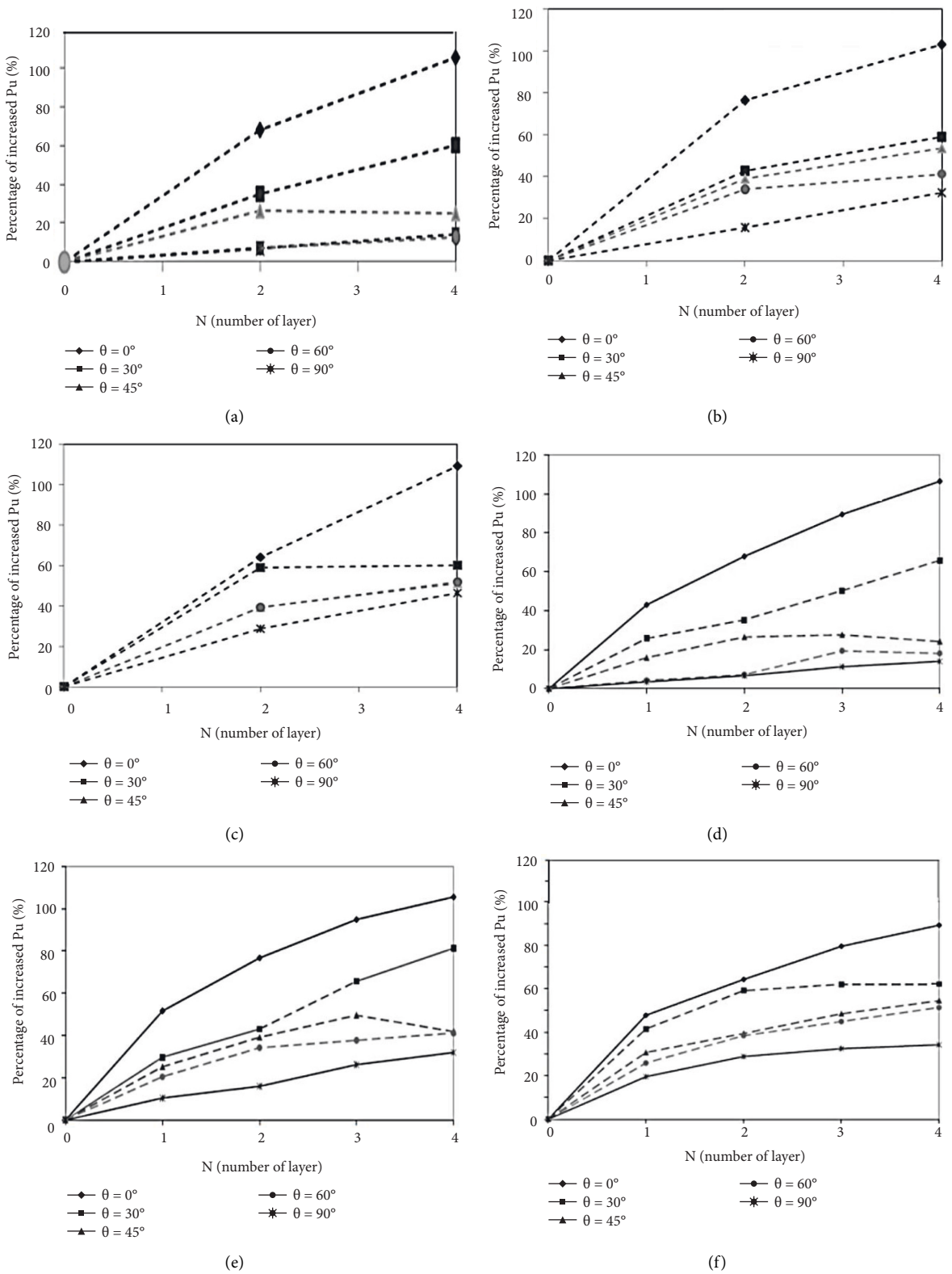

Figure 8: Relationship between number of layers and % Pu increase for long PC beams in different fiber orientations. (a) R-beam $0.2\sigma_p$. (b) R-beam $0.6\sigma_p$. (c) R-beam σ_p. (d) T-beam $0.2\sigma_p$. (e) T-beam $0.6\sigma_p$. (f) T-beam σ_p.

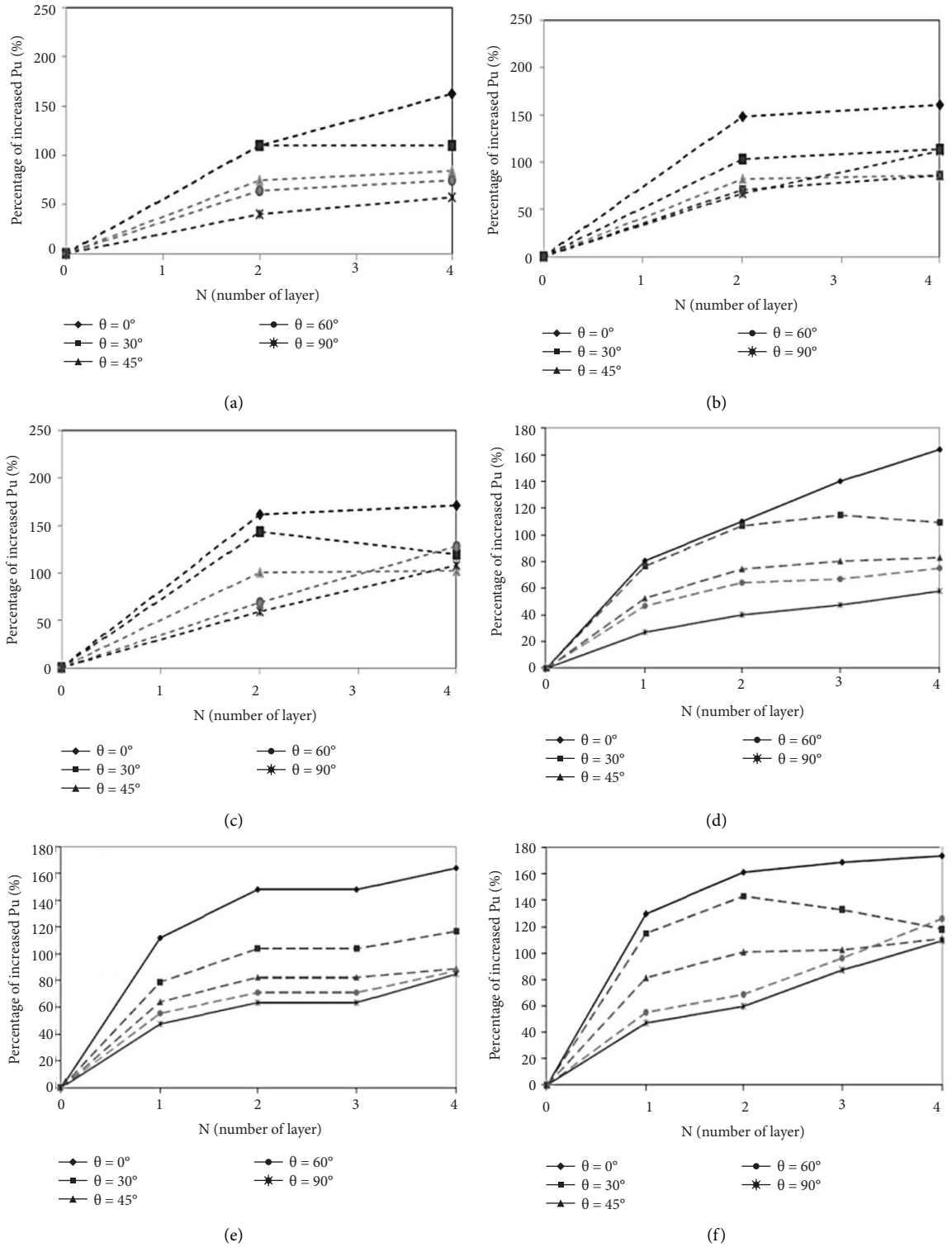

Figure 9: Relationship between number of layers and % Pu increase for long PC beams in different fiber orientations. (a) R-beam $0.2\sigma_p$. (b) R-beam $0.6\sigma_p$. (c) R-beam σ_p. (d) T-beam $0.2\sigma_p$. (e) T-beam $0.6\sigma_p$. (f) T-beam σ_p.

The best fiber orientation is 0 degrees for both long and short beams since, in all cases, it always has a higher percentage of maximum load. The benefits of FRP can significantly increase the ultimate strength of prestressed concrete beams whether the FRP is attached at the bottom or on both sides of the beams.

4. Conclusions

The analysis of the behavior of PC beams strengthened by FRP for both rectangular and T-shape is presented in this paper. The FRP can significantly increase the stiffness as well as the ultimate strength of RCT-beams. A parametric study of this based on nonlinear finite element analyses leads to the following conclusions:

(1) Within the similar dimension of width and height, the maximum loads of T-beams with rectangular beams are slightly higher. The higher maximum loads and displacement can be obtained by considering the flanges in the structure of beam elements. The additional FRP layers would have significant effects on increasing the maximum load, especially for long beams.

(2) The failure of beams is affected by the length of beams and the amount of reinforcement. The cracks mainly occur at the mid-bottom of the beams, which indicates the occurrence of bending failure for the long beams while the cracks for the short beams mainly occur at the support. The increased prestressed load reduced the cracks in the mid-bottom and increased the cracks at the support. The different amounts of reinforcement generate a combination of the failure with other failure modes, such as flexural shear failure.

(3) Different fiber orientations give different results in strengthening PC beams, and the increased number of layers has a greater impact on the effect of fiber orientation to increase the maximum load. However, the best fiber orientation is still 0 degrees.

Data Availability

The data used to support the study are available upon request.

Conflicts of Interest

The authors declare that they have no conflicts of interest.

References

[1] J. Teng, J. Chen, S. Smith, and L. Lam, *FRP Strengthened RC Structures*, John Wiley & Sons, Hoboken, NJ, USA, 2002.

[2] Aci Committe 440 2002, *State-of-the-Art Report on Fiber Reinforced Plastic (FRP) Reinforcement for Concrete Structures*, American Concrete Institute, Farmington Hills, MI, USA, 2002.

[3] A. Nanni, "North American design guidelines for concrete reinforcement and strengthening using FRP: principles, applications and unresolved issues," *Construction and Building Materials*, vol. 17, no. 6-7, pp. 439–446, 2003.

[4] G. M. Chen, J. F. Chen, and J. G. Teng, "On the finite element modelling of RC beams shear-strengthened with FRP," *Construction and Building Materials*, vol. 32, pp. 13–26, 2012.

[5] A. C. I. Committee 318, *Building Code Requirements for Structural Concrete and Commentary (ACI 318-19)*, ACI Committee 318, Detroit, MI, USA, 2019.

[6] H. Kupfer, H. K. Hilsdorf, and H. Rusch, "Behavior of concrete under biaxial stresses," *ACI Structural Journal*, vol. 66, pp. 656–666, 1969.

[7] L. Saenz, "Discussion of "equation for the stress-strain curve of concrete" by Desayi P and Krishnan S," *ACI Structural Journal*, vol. 61, pp. 1229–1235, 1964.

[8] H. T. Hu and W. C. Schnobrich, "Constitutive modeling of concrete by using nonassociated plasticity," *Journal of Materials in Civil Engineering*, vol. 1, no. 4, pp. 199–216, 1989.

[9] H. T. Hahn and S. W. Tsai, "Nonlinear elastic behavior of unidirectional composite laminae," *Journal of Composite Materials*, vol. 7, no. 1, pp. 102–118, 1973.

[10] R. D. Mindlin, "Influence of rotatory inertia and shear on flexural motions of isotropic, elastic plates," *Journal of Applied Mechanics*, vol. 18, no. 1, pp. 31–38, 1951.

[11] S. W. Tsai and E. M. Wu, "A general theory of strength for anisotropic materials," *Journal of Composite Materials*, vol. 5, no. 1, pp. 58–80, 1971.

[12] R. Narayanaswami and H. M. Adelman, "Evaluation of the tensor polynomial and Hoffman strength theories for composite materials," *Journal of Composite Materials*, vol. 11, no. 4, pp. 366–377, 1977.

[13] R. E. Rowlands, *Strength (Failure) Theories and Their Experimental Correlation*, Springer, Berlin, Germany, 1985.

[14] C. Lesmana and H.-T. Hu, "Nonlinear finite element analysis of rectangular reinforced concrete slabs strengthened by fiber reinforced plastics," *Scientia Iranica Transactions A: Civil Engineering*, vol. 22, pp. 615–628, 2015.

[15] H.-T. Hu, F.-M. Lin, H.-T. Liu, Y.-F. Huang, and T.-C. Pan, "Constitutive modeling of reinforced concrete and prestressed concrete structures strengthened by fiber-reinforced plastics," *Composite Structures*, vol. 92, no. 7, pp. 1640–1650, 2010.

[16] I. N. C. Abaqus, *Abaqus Analysis User's Manuals and Example Problems Manuals, Version 6.12*, Academic Press, Cambridge, MA, USA, 2012.